



# A corrosion model for the interpretation of cyclic behavior of reinforced concrete sections

Davide Lavorato<sup>1</sup> | Gabriele Fiorentino<sup>1</sup> | Angelo Pelle<sup>1</sup> |  
Alessandro Rasulo<sup>2</sup> | Alessandro Vittorio Bergami<sup>1</sup> | Bruno Briseghella<sup>3</sup> |  
Camillo Nuti<sup>1,3</sup>

<sup>1</sup>Department of Architecture, Roma Tre University, Rome, Italy

<sup>2</sup>Department of Civil and Mechanical Engineering, University of Cassino and Southern Lazio, Cassino, Italy

<sup>3</sup>College of Civil Engineering, Fuzhou University, Fuzhou, Fujian, China

## Correspondence

Camillo Nuti, Department of Architecture, Roma Tre University, Largo G. B. Marzi 10, 00153, Roma, Italy.  
Email: camillo.nuti@uniroma3.it

## Abstract

A generalized cyclic steel model characterized by isotropic and kinematic hardening, inelastic buckling in compression and corrosion of rebars in reinforced concrete (RC) structures is presented. The model has been implemented in a fiber code, to perform seismic analyses of RC sections. The model is particularly accurate with respect to experimental cyclic behavior of rebars with buckling in compression when the strain does not exceed 1.5%. Twelve configurations of RC cross sections were selected as case studies for three geometries and different steel arrangements, assumed representative of RC columns or bridge piers (in a suitable scale). Each section was subjected to two groups of cyclic curvature histories representative of severe seismic loads, not far from collapse. Different axial loads and corrosion percentages (no corrosion, moderate, or high) have been selected to perform cyclic parametric analyses. One of the cases was taken from an experimental test on columns, deriving also steel characteristics used in all numerical cases. The results of the comparison among RC sections have been discussed. Numerical results show that the maximum compressive strain for steel rebars is always smaller than 1.5%, therefore the proposed steel model is accurate and represents a valid tool for structural assessment. Corrosion reduces RC section capacity, affecting various rebar mechanical characteristics, in particular buckling behavior.

## KEYWORDS

buckling, corroded rebars, corrosion, cyclic steel model, RC structures, seismic response

## 1 | INTRODUCTION

Reinforced Concrete (RC) structures are subjected to degradation phenomena during their service life, one of the main causes being the corrosion of steel reinforcement,

which brings to a reduction of the structural capacity, especially for lack of or improper maintenance interventions, design errors and construction defects.<sup>1–3</sup>

Carbonation and high chloride concentrations are the main causes of rebar corrosion. While carbonation leads to uniform bar section reduction, localized corrosion mechanisms, such as pitting, can arise in RC elements in chloride-containing environments,<sup>4</sup> bringing to a nonuniform reduction of the rebar area.

Discussion on this paper must be submitted within two months of the print publication. The discussion will then be published in print, along with the authors' closure, if any, approximately nine months after the print publication.

The so-called average uniform section reduction has, however, a certain degree of irregularity, which changes rebar section in different positions resulting in an eccentricity of the rebar axial load. Therefore, longitudinal rebars are subjected to axial load and bending while inevitable stress concentrations arise. The overall rebar capacity is reduced in terms of axial force in proportion to the new cross section areas and for the presence of bending, while ultimate strain reduces together with an increased buckling attitude.<sup>5</sup> Uniform area reduction of stirrups decreases member shear strength and flexural ductility.<sup>6</sup> Shear strength is reduced due to: (a) lower stirrups yield force; (b) lower plastic distribution of the force among the stirrups, due to reduced ductility of the rebars. Flexural ductility of the corroded members decreases as stirrup confinement is less effective due to: (a) reduction of stirrups yield force and its consequent confinement of concrete sections; (b) reduction of tensile deformation capacity of rebars, with possible premature breakage; (c) formation of a gap between longitudinal and transversal rebars. This latter increases the longitudinal rebar free length (usually equal to stirrups spacing), therefore worsening the buckling attitude of rebars and reducing the effectivity of confinement too. In the event of stirrup breakage, the free length of the intercepted longitudinal reinforcements could even double, this case is not treated here but is relatively straightforward.

Furthermore, pitting corrosion reduces in an ununiform way the rebar sections producing large localized strains due to abrupt bar section reductions. The ductility of the longitudinal rebar decreases reducing the flexural ductility of the RC member.<sup>7,8</sup>

Pitting corrosion, which becomes dominant for high chloride concentrations, enhances dramatically the phenomena described in case of uniform corrosion, in particular ductility capacity becomes very small due to high strain concentration.

Corrosion, especially pitting, has indirect effects on concrete because rust expansion produces tensile stresses with consequent cracking in concrete, and deterioration of the steel-concrete bond quality.<sup>9</sup>

Note that in case of high uniform corrosion percentages there is an inevitable presence of pitting corrosion with all its negative implications.

Structures subjected to repeated cyclic loads, as those located in earthquake-prone regions, are particularly vulnerable to corrosion, due to the smaller monotonic and cyclic ductility capacity resulting in a reduction of energy dissipation and equivalent damping, with possible crises due to low-cycle fatigue with member failure just after few cycles.<sup>10</sup>

Based on the previous considerations, it is important to include corrosion effects to assess RC members and to evaluate properly the structural retrofitting<sup>11-16</sup> The

paper at hand presents an analytical investigation of the hysteretic axial-bending behavior of RC sections in presence of corroded rebars. The analysis is carried out by means of CYRUS-M, a fiber program used to simulate the cyclic behavior of RC sections, developed using Matlab.<sup>17</sup> CYRUS-M assumes perfect bond between concrete and steel rebars. For these latter a generalized numerical model including corrosion is proposed. The model extends, for the case of corroded bars, the one by Monti and Nuti<sup>18</sup> and Zhou et al.,<sup>19,20</sup> describing the cyclic behavior of longitudinal rebars with inelastic buckling in compression. The scope of this investigation is to show the validity of this unified formulation of steel behavior, which allows dealing with the structural section from its construction, in uncorroded state, to its evolution with time in case of corrosion.

In the first part of this paper we determined the variation of mechanical characteristics of rebars as a function of corrosion percentage:  $\Psi = 100 \cdot (m_0 - m) / m_0$  ( $m_0$ : mass of the uncorroded bar;  $m$ : mass of the corroded bar). The number of experimental data available in literature is limited,<sup>6,21-23</sup> among those the two former describe tests on corroded elements where steel reinforcement has similar mechanical characteristics and permit their use as reference for our calibrations.

Eventually, the model parameter variation here derived between the two reference cases seems significant, while dispersion is large even in each of the cases. We decided to use the data from Reference 22 only in the analyses, assuming that each steel has its behavior that must be characterized. Therefore, the present paper represents the state of an ongoing research without pretending to give conclusive results, while there is the need of further experimental tests for what concerns corroded steel parameters.

The generalized numerical model for bar cyclic behavior with buckling in compression including corrosion is then presented.

Without claiming to exhaust the problem, three section geometries, assumed representative of RC columns or bridge piers (in a suitable scale), under cyclic bending and constant axial load are investigated. For every geometry, four different reinforcement quantities are considered, for a total of twelve sections (three section heights and four reinforcement quantities). The different heights of the section intend to explore the maximum strain demand of longitudinal steel rebars.

Two groups of cyclic curvature histories, representing the response under severe earthquake loading conditions, were applied to each section: the first imposes the same maximum curvature ductility demand to each section, while the second imposes the maximum curvatures that brings, in each case of geometry and axial load, steel in

compression to a strain of 1.5%. If this strain is not overtaken, the negative linear assumption of steel stress strain in compression in case of buckling coincides with the experimental evidence resulting very accurate. Comparing the former curvature histories with the latter, it is shown that the strain of 1.5% in compression in real structures is far beyond seismic demand even for very severe seismic input.

The parameters that mainly influence the cyclic behavior of RC sections are the axial load and steel corrosion percentage. The two parameters were varied with two different patterns: (i) fixing a percentage of corrosion and varying the nondimensional axial force on the section  $\nu$  ( $\nu = N/(f_c A_c)$ ,  $f_c$ : concrete compression strength,  $A_c$ : section area  $b \cdot h$ ); (ii) fixing the  $\nu$  value and varying the percentage of corrosion.

The outcomes of the parametric analyses are reported in terms of maximum steel strain in tension and compression, and moment/curvature behavior for the corroded and the uncorroded RC sections are discussed. The validity of the cyclic model for steel with the “simple” linear descending envelope in compression is proved.

## 2 | GEOMETRIES AND MECHANICAL PROPERTIES

Corrosion produces a change in the geometry of steel rebars and their mechanical properties. The equivalent (assuming circular section after corrosion) corroded rebar diameter  $D'$  can be evaluated by Equation (1):

$$D' = D \cdot \sqrt{\left(1 - \frac{m_0 - m}{m_0}\right)} = D \cdot \sqrt{(1 - \Psi/100)} \quad (1)$$

Where  $D$  is the diameter of the uncorroded rebar, while corrosion percentage, as defined in § 1, is:

$$\Psi = \frac{m_0 - m}{m_0} \cdot 100 \quad (2)$$

The mechanical property  $X'_i$  ( $i$  = stress/force/strain) of the corroded rebar in case of corrosion (uniform or pitting) may be expressed as function of the uncorroded bar mechanical property  $X_i$  ( $i$  = stress/force/strain) by Equation (3).

$$X'_i = X_i \cdot (1 - \beta''_i \cdot \Psi) \quad (3)$$

Where  $\beta''_i$  is the coefficient which takes into account uniform or pitting corrosion.<sup>6</sup> The superscript “” for the

parameter  $\beta$  means that the parameter  $X'_i$  refers to the corroded areas (for example the ultimate stresses are the force divided by the corroded area).

As anticipated in §1, we have derived the presented values of  $\beta''_i$  with reference to 21.<sup>22</sup> The experimental load strain curves of the rebar in tension obtained in Reference 21, for different corrosion percentages, are shown in Figure 1a, while the mechanical parameters of the corroded rebar used in this work are defined in Figure 1b.  $f_y$ ,  $f_u$ ,  $f_{max}$ , and  $\epsilon_y$ ,  $\epsilon_u$ ,  $\epsilon_{max}$  are the yield, ultimate and maximum strengths and strains, respectively.  $E_{s0}$  is the initial Young modulus of steel, and  $b_0$  is the hardening ratio.

Figure 2 shows the obtained coefficients  $\beta''_i$  as function of corrosion percentages for  $i = f_y$ ,  $f_{max}$ ,  $\epsilon_{max}$ , and  $b$  (for<sup>22</sup>  $i = f_y$ ,  $f_{max}$  only). In case<sup>21</sup> we have fitted with a constant or with a linear function of  $\Psi$ . Though the mechanical characteristics of reinforcing steel utilized the two test campaign,<sup>21,22</sup> are similar, the derived values of  $\beta''_{f_y}$  and  $\beta''_{f_{max}}$  are very different 400 and 3,000%, respectively for a constant value fit (generally adopted in the technical literature), but even larger for large  $\Psi$  in case of linear fit in Reference 21. On the base of these results we should conclude that the variation with  $\Psi$  could change from steel to steel, however, further experimental results are needed to draw general conclusion.

In the following of this paper we decided to refer to Reference 21, from which we could derive the decay of all parameters. We adopted the linear variation  $\beta''_{f_y} = 0.0011\Psi$ , which, for this data fitting, seems more accurate, with respect to the constant value  $\beta''_{f_y} = 0.20$ . This will have an influence on moment curvature results for large  $\Psi$  values, see §5.

Corrosion reduces the diameters of the longitudinal rebars and the stirrups,  $D$  and  $D_{st}$ , respectively, while a gap  $G$  creates between longitudinal and transversal reinforcement, see Figure 3. Buckling arises, in the compressed longitudinal rebars, when the slenderness  $\lambda = L/D$ , where  $L$  is the free length in compression that is, the distance between the hinges in buckling, is greater than the critical value of the slenderness  $\lambda_{cr}$  [Equation (4)]:

$$\lambda_{cr} = 5 / \sqrt{\frac{f_{y-}}{450}} \quad (4)$$

where  $f_{y-}$  is the yield stress in compression.  $L$  is usually assumed equal to stirrup spacing as stirrups impede transverse movement of rebars. Corrosion increases slenderness as longitudinal rebar can displace laterally of the gap  $G$  until they touch the stirrup, increasing  $L$ :  $L' > L$ , while decreasing  $D$ , thus  $\lambda' > \lambda$ . Figure 3 illustrates this phenomenon on a bridge pier.

The gap  $G$  is given by Equation (5) (see Figure 3):

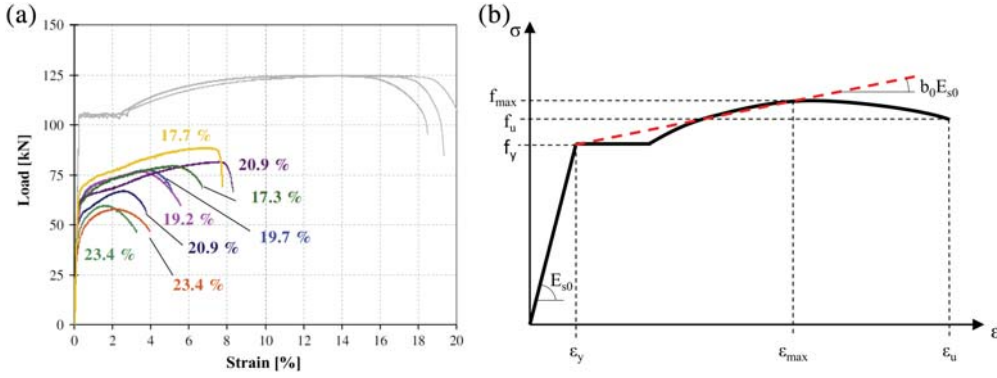


**FIGURE 1** (a) Load-strain curves for corroded rebar in RC members for different corrosion percentages; Picture adapted from Meda et al. 2014<sup>22</sup>; (b) Simplified stress-strain relationship for corroded rebar and mechanical parameters used in this work

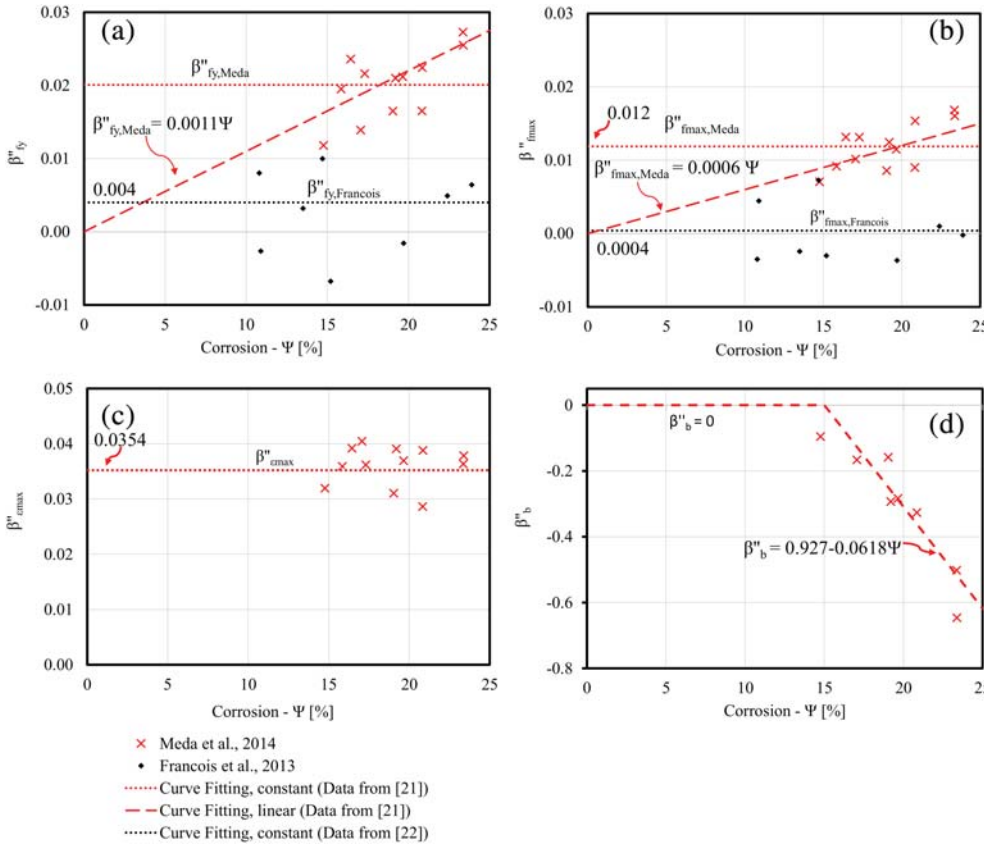


**FIGURE 2** Calibration of  $\beta''I$  with the corrosion percentage  $\Psi$  for different parameters I: (a) yield stress  $f_y$ ; (b) maximum stress  $f_{max}$ ; (c) maximum strain  $\epsilon_{max}$ ; (d) hardening ratio  $b$ . Experimental data from: Meda et al. 2014 (red crosses)<sup>21</sup>; Francois et al. 2013 (black dots).<sup>22</sup> Interpolation curves: Constant and linear fitting to Meda et al. 2014 (dotted and dashed red lines); Constant fitting to Francois et al. 2013 (dotted black lines)

$$G = \frac{(D_{st} - D'_{st})}{2} + \frac{(D - D')}{2} \quad (5)$$

Where  $D_{st}$  and  $D'_{st}$  are the uncorroded and corroded stirrup diameters, respectively. The free length for the corroded rebars  $L'$  can be given by Equation (6)<sup>24</sup>:

$$L' = L + 2 \cdot \mu \cdot G \quad (6)$$

where  $\mu$  is a coefficient greater than 0.

Based on some preliminary evaluations,<sup>24</sup> it is assumed as first guess that  $\mu = 5$  (though additional evaluations should be carried out as at the moment no papers exist on the topic).

From Equation (4), for the corroded rebar, the critical slenderness  $\lambda'_{cr}$  is given by Equation (7):

$$\lambda'_{cr} = 5 / \sqrt{\frac{f'_{y-}}{450}} \quad (7)$$

where  $f'_{y-}$  is the yield stress of the corroded rebar in compression. Note that usually yielding stress  $f'_{y-}$  reduces with corrosion percentage  $\Psi$ , therefore  $\lambda'_{cr} > \lambda_{cr}$ .

Figure 4 shows the slenderness  $\lambda'$  and  $\lambda'_{cr}$  as function of the corrosion percentage  $\Psi$  in case  $\mu = 0, 1, 3, 5, 7$  in Equation (6), for a stirrup spacing of 70 mm. One can note that buckling can be excluded for  $\Psi < 5\%$ , as  $\lambda' < \lambda'_{cr}$ . When corrosion percentage increases and varies



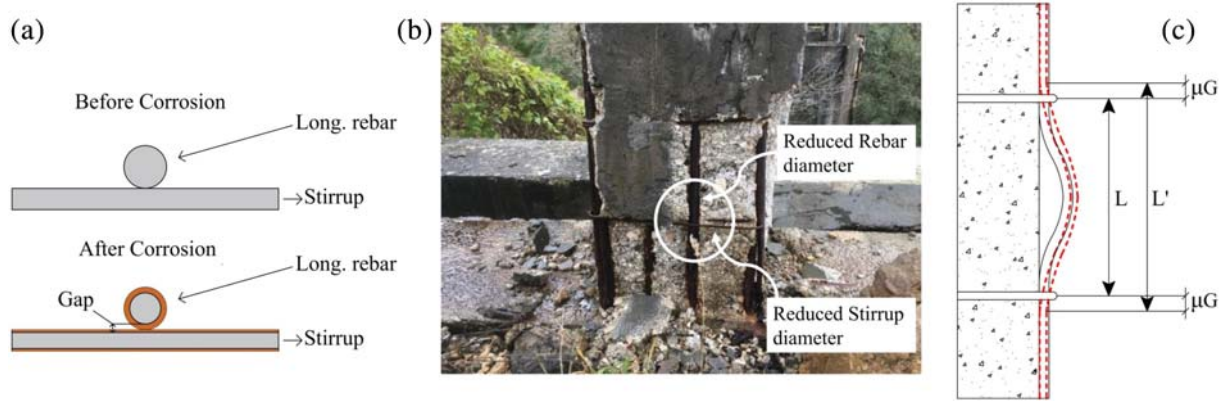


**FIGURE 3** (a) Scheme of Gap  $G$  between stirrups and longitudinal rebars, in brown is the eliminated steel for the effect of corrosion; (b) Corrosion on a bridge pier with gap formation; (c) rebar buckling mechanism: uncorroded (solid black line) and corroded (dashed red line) rebar

between 5 and 18%, the value of  $\lambda'_{cr}$  slightly increases, however less than  $\lambda'$  for  $\mu = 5, 7$  for which buckling arises. To investigate the effect of  $\mu$ , one can see in Figure 4 that for  $\mu = 1$  or 3 buckling never happens, while for values larger than  $\mu = 5$  corrosion leads to buckling. The effect of the gap between stirrup and longitudinal rebars seems worth to be investigated in future works.

On the other hand it has to be highlighted that the level of uncertainty for high corrosion values is very high, therefore one should be cautious to consider the positive effect of yielding stress reduction with respect to buckling (Equation (7)) and the effect of the gap, previously described, should be taken into account.

### 3 | CYCLIC MODEL FOR CORRODED REBARS AND RC SECTION ANALYSIS

The authors of the present paper proposed a generalized cyclic steel model characterized by isotropic and kinematic hardening with possible inelastic buckling in compression.<sup>18,19</sup>

Basically, the model defines the envelope skeleton curve, constituted by straight segments, with elastic and plastic branches, characterized by the  $E$  modulus and hardening  $b$ , intersecting in the yielding ( $\epsilon_y^n, f_y^n$ ) and inversion ( $\epsilon_r^{n-1}, f_r^{n-1}$ ) points, respectively.

Buckling arises, in the compressed longitudinal rebars, when the slenderness  $\lambda > \lambda_{cr}$ , in this case  $b$  is negative.

The skeleton curves represent the asymptotes of loading and reloading curves (RLCs), starting from the inversion points. RLCs are of the well-known Menegotto-Pinto type,<sup>25</sup> given by Equations (8) and (9):

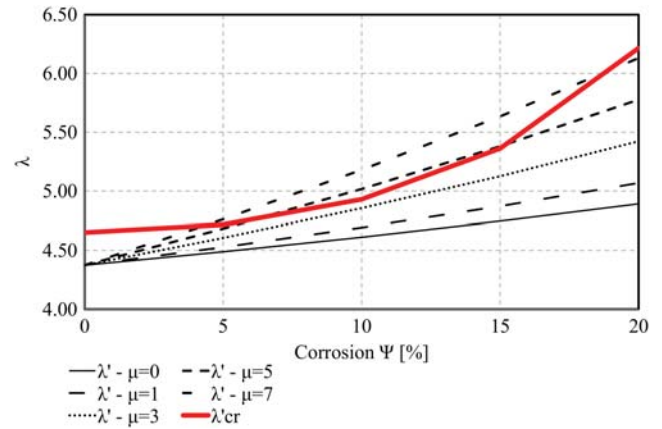


**FIGURE 4** Slenderness  $\lambda$  (stirrup spacing 70 mm) for different corrosion percentages and  $\mu = 0, 1, 3, 5, 7$ ;  $\lambda'_{cr}$  for different corrosion percentages

$$\sigma^* = b^n \cdot \epsilon^* + \frac{(1 - b^n) \cdot \epsilon^*}{\left(1 + e^{*R^n}\right)^{\frac{1}{R^n}}} \quad (8)$$

Where:

$$\sigma^* = \frac{(\sigma - f_r^{n-1})}{(f_y^n - f_r^{n-1})}; \quad \epsilon^* = \frac{(\epsilon - \epsilon_r^{n-1})}{(\epsilon_y^n - \epsilon_r^{n-1})} \quad (9)$$

$n$  is the half loading cycle number,  $R^n$  the parameter that governs the transition from the elastic to inelastic branch, the smaller  $R^n$  the smoother is the transition.

The yielding points of the skeleton curves vary according to the hardening rules, kinematic and isotropic, described in Reference 19 with the evolution described in Reference 20 including for example possible anisotropy in tension and compression. The  $E^n$  modulus, when downloading from compression, as well as the hardening value  $b^n$  (ratio between  $E$  modulus in before and after yielding) vary with load history. The parameter  $R^n$  depends on the

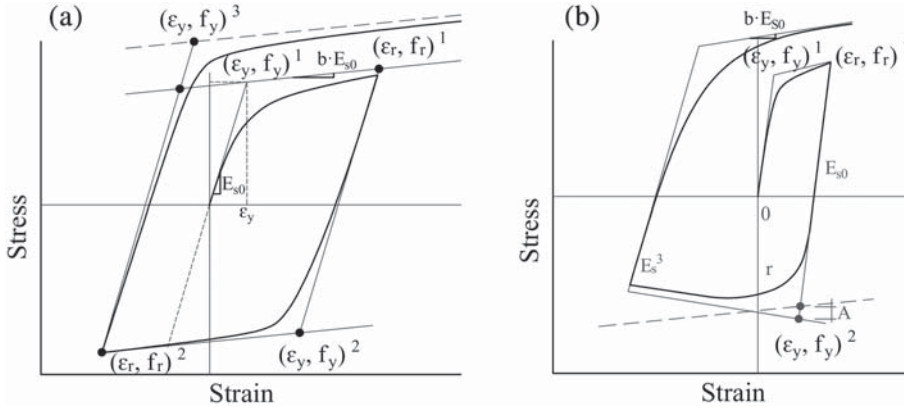


**FIGURE 5** Reference steel model<sup>20</sup>: (a) curve without buckling; (b) curve with buckling

maximum plastic excursion during the strain history and the initial value  $R_0$ .  $R^n$  has different formulations for unloading (from tension to compression) and reloading (from compression to tension) branches.

The evolution expressions of the different parameters differ in presence of buckling. The updating expression of  $f_y^n$  for each branch  $n$  by Equation (10):

$$f_y^n = \left| f_y^1 \right| \cdot \text{sign} \left( -\xi_p^{n-1} \right) + P \cdot \Delta \sigma_K^{n-1}(\cdot) + (1-P) \cdot \Delta \sigma_I^{n-1}(\cdot) \cdot \text{sign} \left( -\xi_p^{n-1} \right) \quad (10)$$

Where  $\text{sign}(x)$  is the sign function,  $P$  is the weight coefficient ( $p = 1$ ) for the two hardening contributions,  $\Delta \sigma_K^n$  is the kinematic hardening contribution and  $\Delta \sigma_I^n$  is the isotropic hardening contribution for the branch  $n$ . In absence of buckling they both depend on  $b^n$ ,  $E^n$ , and the former hardening on the plastic excursion  $\xi_p^n$  while the latter on the additional plastic excursion  $\gamma_p^n$ . In presence of buckling the dependence on  $\xi_p^n$  and  $\gamma_p^n$  is exchanged between  $\Delta \sigma_K^n$  and  $\Delta \sigma_I^n$ . Note that  $b^n$  depends on  $b^1$ ,  $\gamma_p^n$ ,  $f_y^1$ ,  $E_0$  and, in case of buckling, on the plastic work  $\Phi_p^n$  too.

The details of the model are given in the Appendix S1, while some of the major characteristics are shown in Figure 5a,b.

The model is very accurate if the strain in compression is smaller than 1.5%. For larger values in compression the accuracy is partially reduced as a nonlinear curve better describes the behavior of the rebar.<sup>26</sup> However, larger deformation values can hardly be reached in real concrete sections.

The model, with the same formulation, is extended to simulate the hysteretic behavior of corroded rebars in reinforced concrete structures.

In a rebar with the new reduced  $D'$ , due to corrosion, two main parameters changes: the yield stress  $f_y^1$  and

hardening ratio  $b_o^1$ . They can be derived from the uncorroded characteristics by Equations (11) and (12) based on Equation (3):

$$f_y^1 = f_y^1 \cdot \left( 1 - \beta_{f_y}''(\Psi) \cdot \Psi \right) \quad (11)$$

$$b_o^1 = b_o^1 \cdot \left( 1 - \beta_b''(\Psi) \cdot \Psi \right) \quad (12)$$

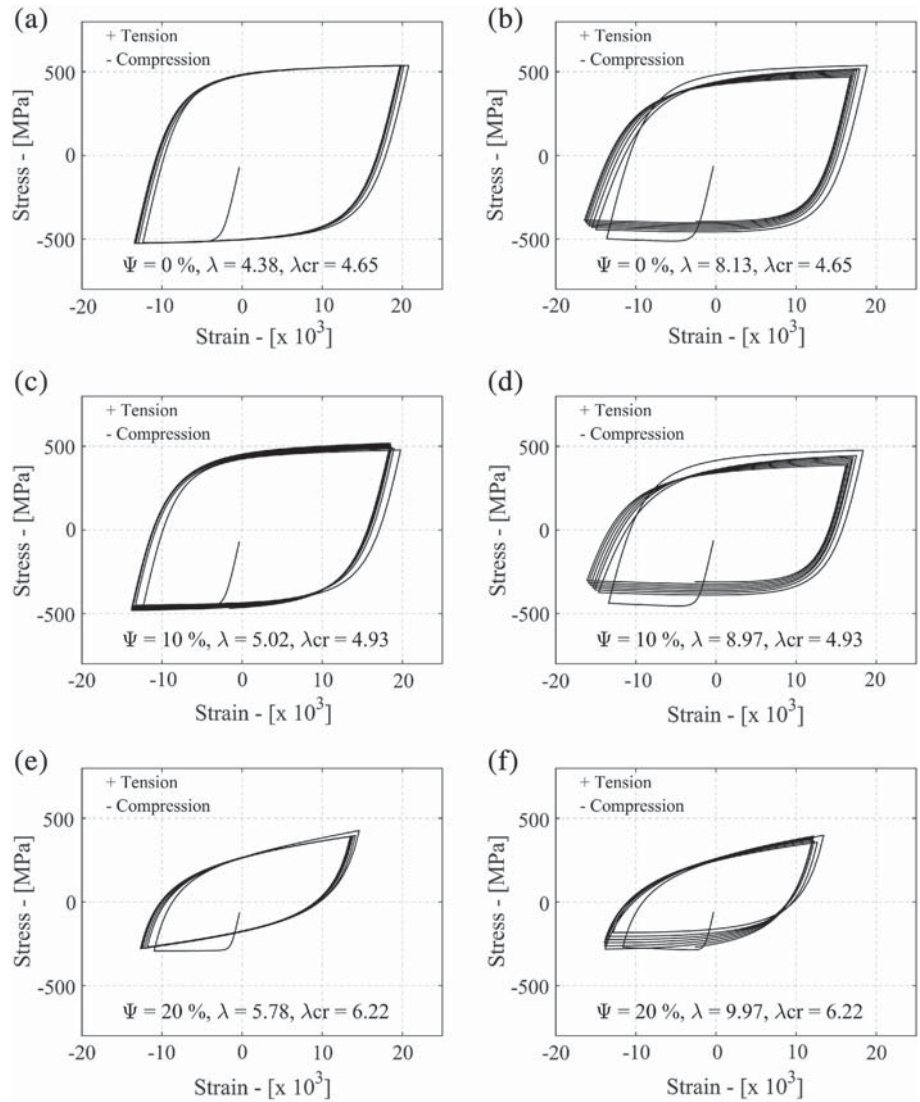
where  $f_y^1$  and  $b_o^1$  are the yield stress and the hardening ratio for the uncorroded rebars,  $\beta_{f_y}''(\Psi)$  and  $\beta_b''(\Psi)$  are the coefficients provided in Figure 2 for a given  $\Psi$ . It is worth mentioning that the values of parameters  $f_y^1$  and  $b_o^1$  for pitting corrosion could be different in tension and compression. Due to the limited data available, in this work it is assumed that this variation is the same in compression and tension while the effect of corrosion on the parameter  $R$  was not investigated.

The new values must be introduced in Equation (10), therefore  $f_y^1$  and  $b_o^1$  will change, this latter affecting  $\Delta \sigma_K^n$  and  $\Delta \sigma_I^n$  and  $R$ .

The in-house software CYRUS-M (CYclic Response of Upgraded Sections) was implemented in Matlab<sup>17</sup> to perform cyclic analysis of the section, discretized into uniaxial fibers under the hypothesis of: (a) plain sections, (b) perfect steel-concrete bond. The rebars were modeled using the hereby proposed generalized steel model including corrosion, concrete fibers are modeled by the modified Kent and Park<sup>27</sup> model: unconfined concrete for concrete cover and confined concrete for the core.

The program applies the fixed vertical axial load on the section and imposes a cyclic curvature history on the section obtaining the corresponding moment for each imposed curvature value. The program outputs are given in terms of moment-curvature and fiber stress-strain histories, as shown in Figure 6 for different cases with and without buckling.

**FIGURE 6** Stress–strain behavior obtained with Cyrus-M for the RC section  $300 \times 500 \text{ mm}^2$  with  $\nu = 26\%$ ,  $\rho = 0.9\%$  with curvature histories reported in Table 5. Group 2 analyses, same ductility in curvature: (a)  $\Psi = 0\%$ ,  $s = 70 \text{ mm}$ ; (b)  $\Psi = 0\%$ ,  $s = 130 \text{ mm}$ ; (c)  $\Psi = 10\%$ ,  $s = 70 \text{ mm}$ ; (d)  $\Psi = 10\%$ ,  $s = 130 \text{ mm}$ ; (e)  $\Psi = 20\%$ ,  $s = 70 \text{ mm}$ ; (f)  $\Psi = 20\%$ ,  $s = 130 \text{ mm}$ . Rebar nominal diameter: 16 mm



## 4 | PARAMETRIC INVESTIGATION

### 4.1 | Case studies and parametric analyses

The parametric cyclic analysis consisted of three sections, with different reinforcements at various corrosion levels, under two groups of cyclic curvature histories.

Axial force and corrosion percentages were varied with two different patterns: (i) fixed nondimensional axial load  $\nu$  equal to 26%, the value of the test in Reference 21, for different steel corrosion percentage values ( $\Psi = 0, 10, 20\%$ ); (ii) fixed steel corrosion percentage:  $\Psi = 20\%$  and for different nondimensional axial load ( $\nu = 0, 7, 13, 26\%$ ).

Note that for the section  $300 \times 300 \text{ mm}^2$ ,  $\nu = 0, 7, 13$ , and 26% correspond to the axial forces 0, 100, 200, and 400 kN, this latter being the axial load on the columns tested in Reference 21.

### 4.2 | Geometries of the sections and corresponding fiber models

The analysis considers three different rectangular cross sections, with two different percentages of longitudinal reinforcement and two different stirrups spacings (same stirrups diameter) for a total of 12 RC cases. The three rectangular sections are:  $300 \times 300$ ,  $300 \times 500$ , and  $300 \times 1,200 \text{ mm}^2$ . These sections have the same width but different height to increase the maximum strain demand on the longitudinal steel rebars, for a given curvature. Two different longitudinal steel geometric percentages were selected, representative of existing RC column or bridge pier (in a suitable scale):  $\rho = 0.9$  or 2.7%.

Two longitudinal rebar slenderness:  $L/D = 8.13$  and  $L/D = 4.38$  (the critical slenderness being 4.65 for  $f_y = 520 \text{ Mpa}$ , Equation (4)), correspond to cases with or without buckling of the rebar in compression.

Table 1 reports the 12 cases that were analyzed and Figure 7 the design schematic (no details of ties and

reinforcements along the vertical sides) drawings of the selected sections. Figure 8 shows the fiber models adopted for three cross sections investigated. Each section is divided into steel (green circles) and concrete fibers (red rhombuses for the confined concrete fibers; blue crosses for the unconfined concrete fibers). The concrete fibers at the section corners were removed to simulate the concrete cover spalling due to rust expansion.

**TABLE 1** Cases of study: different configurations used in the analyses

Section #	$b$ (mm)	$h$ (mm)	$\rho$	Spacing (mm)
1	300	300	0.9	70
2	300	300	2.7	70
3	300	300	0.9	130
4	300	300	2.7	130
5	300	500	0.9	70
6	300	500	2.7	70
7	300	500	0.9	130
8	300	500	2.7	130
9	300	1,200	0.9	70
10	300	1,200	2.7	70
11	300	1,200	0.9	130
12	300	1,200	2.7	130

The materials characteristics obtained derived for this study from the experimental tests of Meda et al.,<sup>21</sup> typical of existing RC structures, are given in Table 2.

### 4.3 | Deformation histories

Each section was subjected to two groups of cyclic curvature histories representative of severe seismic loads: History 1 (IC1) imposes the same curvature ductility demand to each section; History 2 (IC2) imposes the maximum curvatures so that the maximum compressive strain of the rebar is always equal to 1.5% (compressive strain limit of the steel model to be accurate). Curvatures of Group 2 are much larger than those imposed in Group 1. Each imposed curvature history is formed by six symmetric cycles (Figure 9), note that Eurocode 8 part 2 for bridges considers at least five cycles for stability.<sup>28</sup>

The imposed curvatures History 1: IC1, derived from Reference 21. In that paper the column drift corresponding to the collapse of the corroded column is 2.5%. Experimental curvatures were given for the case of uncorroded element only (not for the corroded one). We derived the ductility that we imposed: IC1, for the  $300 \times 300$  section, dividing the given curvatures by the yield curvature estimated by Equation (13)<sup>29</sup>:

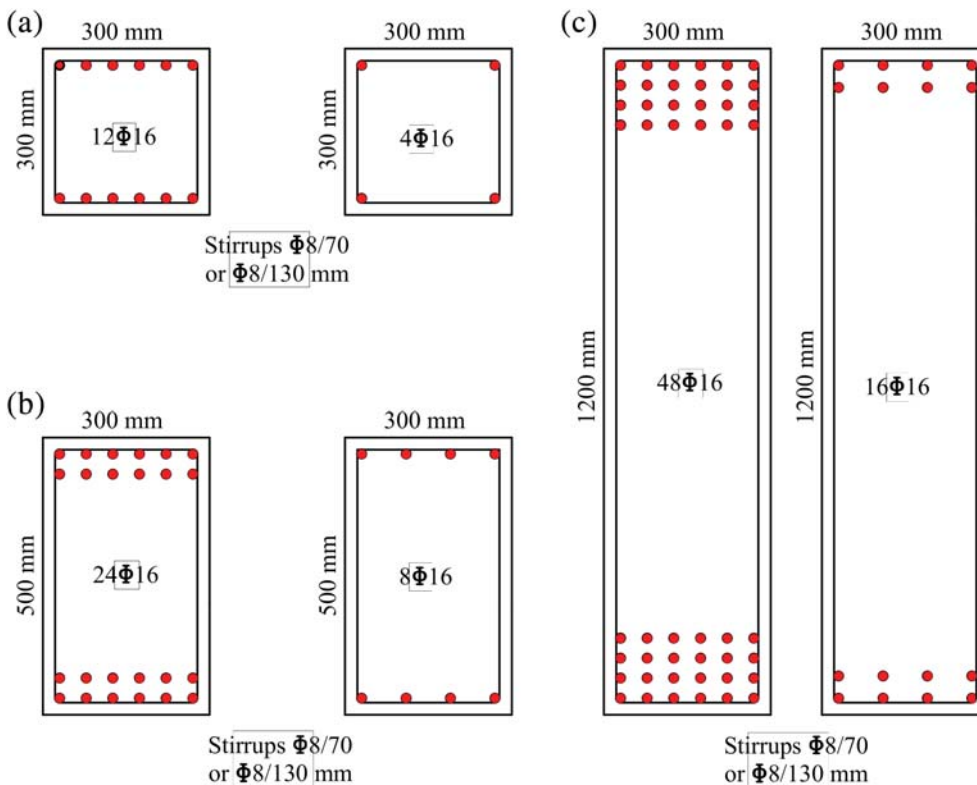


**FIGURE 7** RC sections selected (schematic) as the cases of study: (a)  $300 \times 300$  mm<sup>2</sup>; (b)  $300 \times 500$  mm<sup>2</sup>; (c)  $300 \times 1,200$  mm<sup>2</sup>, each one for  $\rho = 0.9$  or 2.7%



$$\chi_y = 2.3 \frac{\varepsilon_{sy}}{d} \quad (13)$$

where  $\varepsilon_y$  is the yield strain of the longitudinal rebars, reported in Table 1, and  $d$  is the effective depth of the section. The obtained ductility is 3.26.

The same maximum curvature ductility per cycle was applied to all sections.

Note that for the same steel type, the yield curvature depends on  $d$  (effective depth of the section) and

corrosion percentage, as in each section corrosion reduces the yield strain  $\varepsilon_y$ . For this reason, the curvature demand of IC1 is different for each section in function of  $d$  and of the corrosion percentage, even if the ductility demand is the same for all cases. The different imposed curvatures are given in Table 3 for corrosion percentage  $\Psi = 20\%$  and varying axial load  $\nu$  and in Table 4 for  $\nu = 26\%$  and varying  $\Psi$ .

Regarding IC2, the maximum curvatures applied on the sections, those which produce a compression deformation of 1.5%, are given in Table 5 for the different sections and values of corrosion. Note that IC2 investigates different section ductility demands with values of ductility from six to more than eight, much larger than for IC1. IC2 curvatures are far beyond those at failure for the corroded structures, at least on the base of the tests in Reference 21.

## 5 | ANALYSES RESULTS

Results are shown starting from the imposed deformation history IC1, which imposes a maximum curvature similar to the tests,<sup>21</sup> extending the analysis to other corrosion levels and other section geometries too. After maximum strains the cyclic moment curvatures are shown. Then the same results for IC2, which imposes larger demands, are shown.

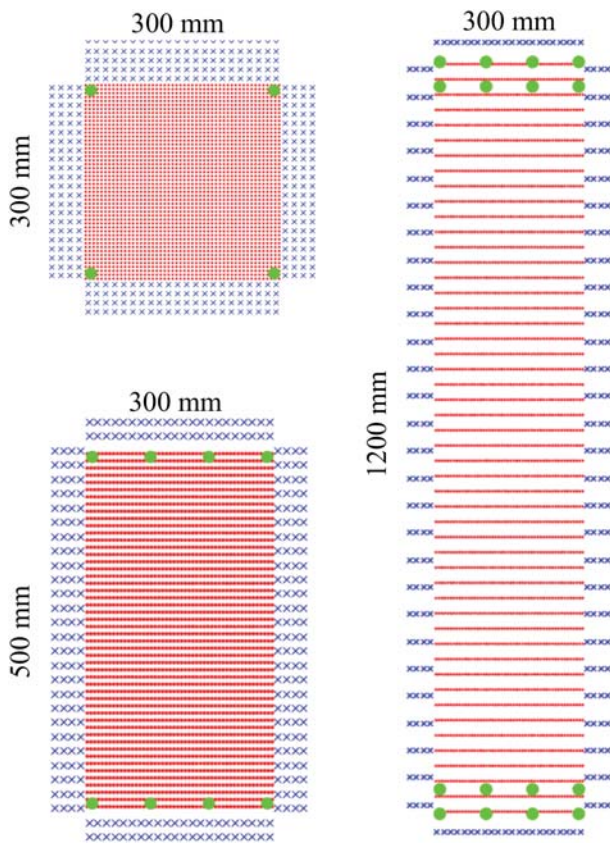


**FIGURE 8** Fiber model implemented in CYRUS-M for corroded sections; (a)  $300 \times 300 \text{ mm}^2$ ; (b)  $300 \times 500 \text{ mm}^2$ ; (c)  $300 \times 1,200 \text{ mm}^2$  for  $\rho = 0.9\%$  and  $\Psi = 20\%$ . Red rhombuses: confined concrete fibers; blue crosses: unconfined concrete fibers; steel: green circles

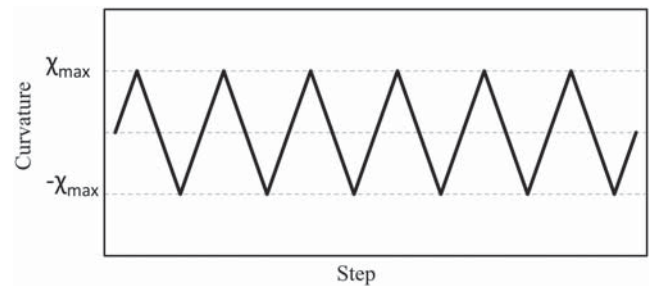


**FIGURE 9** Example of curvature history applied on the sections for each parametric analysis

**TABLE 2** Material properties for the cases of study (MPa)

Unconfined concrete	Steel (uncorroded— $\Psi = 0\%$ )	Steel (corroded— $\Psi = 10\%$ )	Steel (corroded— $\Psi = 20\%$ )
$f_c = 17.0$	$f_y = 520.0$	$\beta''_{fc} = 1.10 \cdot 10^{-2}$	$\beta''_{fc} = 2.20 \cdot 10^{-2}$
$\varepsilon_c = 2.0 \%$	$f_{max} = 620.0$	$f'_y = 462.8$	$f'_y = 291.2$
$E_c = 30,000$	$b = 0.0035$	$\varepsilon_y = 2.2 \%$	$\varepsilon_y = 1.3 \%$
	$\varepsilon_u = 14\%$	$\varepsilon_u = 8.8\%$	$\varepsilon_u = 4.1\%$
	$E_{s0} = 210,000$	$E_{s0} = 210,000$	$E_{s0} = 210,000$

Section	$\nu$ (%)	$\chi_{\max}$ (1/mm)	$\chi_y$ (1/mm)	$\mu_x$
300 × 300	0–6.5 to 13–26	6 (+4.35E–05 –4.35E–05)	1.33E–05	3.26
300 × 500	0–6.5 to 13–26	6 (+2.46E–05 –2.46E–05)	7.54E–06	3.26
300 × 1,200	0–6.5 to 13–26	6 (+9.74E–06 –9.74E–06)	2.99E–06	3.26

**TABLE 3** Group 1 analyses: Curvature history for  $\Psi = 20\%$  and varying normalized axial load  $\nu$

Section	$\Psi$ (%)	$\chi_{\max}$ (1/mm)	$\chi_y$ (1/mm)	$\mu_x$
300 × 300	0	6 (+7.14E–05 to 7.14E–05)	2.19E–05	3.26E+00
	10	6 (+6.83E–05 to 6.83E–05)	2.09E–05	3.26E+00
	20	6 (+4.35E–05 to 4.35E–05)	1.33E–05	3.26E+00
300 × 500	0	6 (+4.04E–05 to 4.04E–05)	1.24E–05	3.26E+00
	10	6 (+3.86E–05 to 3.86E–05)	1.18E–05	3.26E+00
	20	6 (+2.46E–05 to 2.46E–05)	7.54E–06	3.26E+00
300 × 1,200	0	6 (+1.60E–05 to 1.60E–05)	4.91E–06	3.26E+00
	10	6 (+1.53E–05 to 1.53E–05)	4.69E–06	3.26E+00
	20	6 (+9.74E–06 to 9.74E–06)	2.99E–06	3.26E+00

**TABLE 4** Group 1 analyses: Curvature history for  $\nu = 26\%$  and varying corrosion percentage  $\Psi$

Section	$\Psi$ (%)	$\chi_{\max}$ (1/mm)	$\chi_y$ (1/mm)	$\mu_x$
300 × 300	0	6 (+1.45E–04 to 1.45E–04)	2.19E–05	6.62
	10	6 (+1.35E–04 to 1.35E–04)	2.09E–05	6.45
	20	6 (+1.10E–04 to 1.10E–04)	1.33E–05	8.25
300 × 500	0	6 (+8.20E–05 to 8.20E–05)	1.24E–05	6.62
	10	6 (+8.00E–05 to 8.00E–05)	1.18E–05	6.76
	20	6 (+6.50E–05 to 6.50E–05)	7.54E–06	8.63
300 × 1,200	0	6 (+3.20E–05 to 3.20E–05)	4.91E–06	6.52
	10	6 (+2.95E–05 to 2.95E–05)	4.69E–06	6.29
	20	6 (+2.60E–05 to 2.60E–05)	2.99E–06	8.70

**TABLE 5** Group 2 analyses: Curvature history for  $\nu = 26\%$  and varying corrosion percentage  $\Psi$

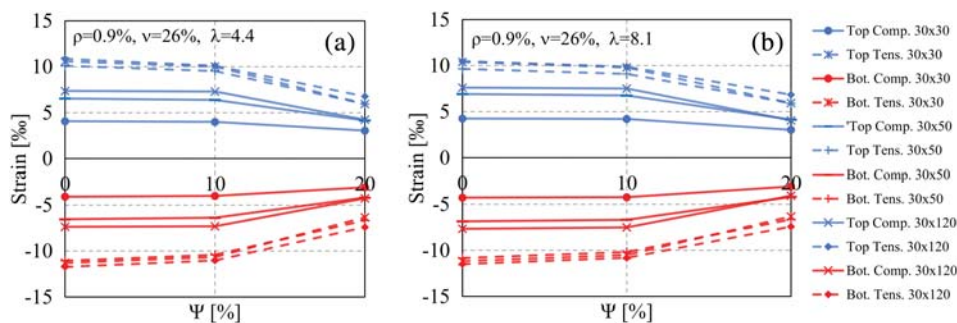


**FIGURE 10** Load History IC1. Stirrup spacing  $s = 70$  mm, Slenderness  $\lambda = 4.4$  (a),  $s = 130$  mm,  $\lambda = 8.1$  (b). Reinforcement ratio  $\rho = 0.9\%$ . Maximum strains of steel fibers for ( $\nu, \Psi$ , pattern (i)): normalized axial load  $\nu = 26\%$ , and different values of the corrosion percentage:  $\Psi = 0, 10, 20\%$ . Rebars in compression (Comp.), continuous lines; Rebars in tension (Tens.), dotted lines; Top reinforcement (Top); Bottom reinforcements (Bot)

Figure 10 shows the results of the analyses under IC1 (i.e., same curvature ductility demand) for parameter pattern (i) in §4.1, stirrups spacings  $s$ : 70 mm (Figure 10a)

and 130 mm (Figure 10b). The results are in terms of maximum strain of the steel rebars, both in compression and in tension.

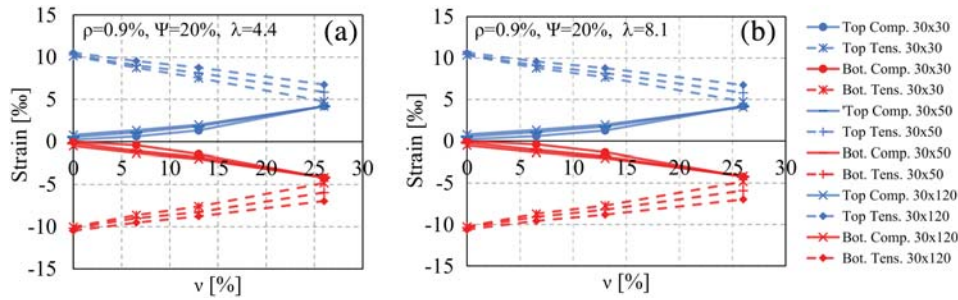
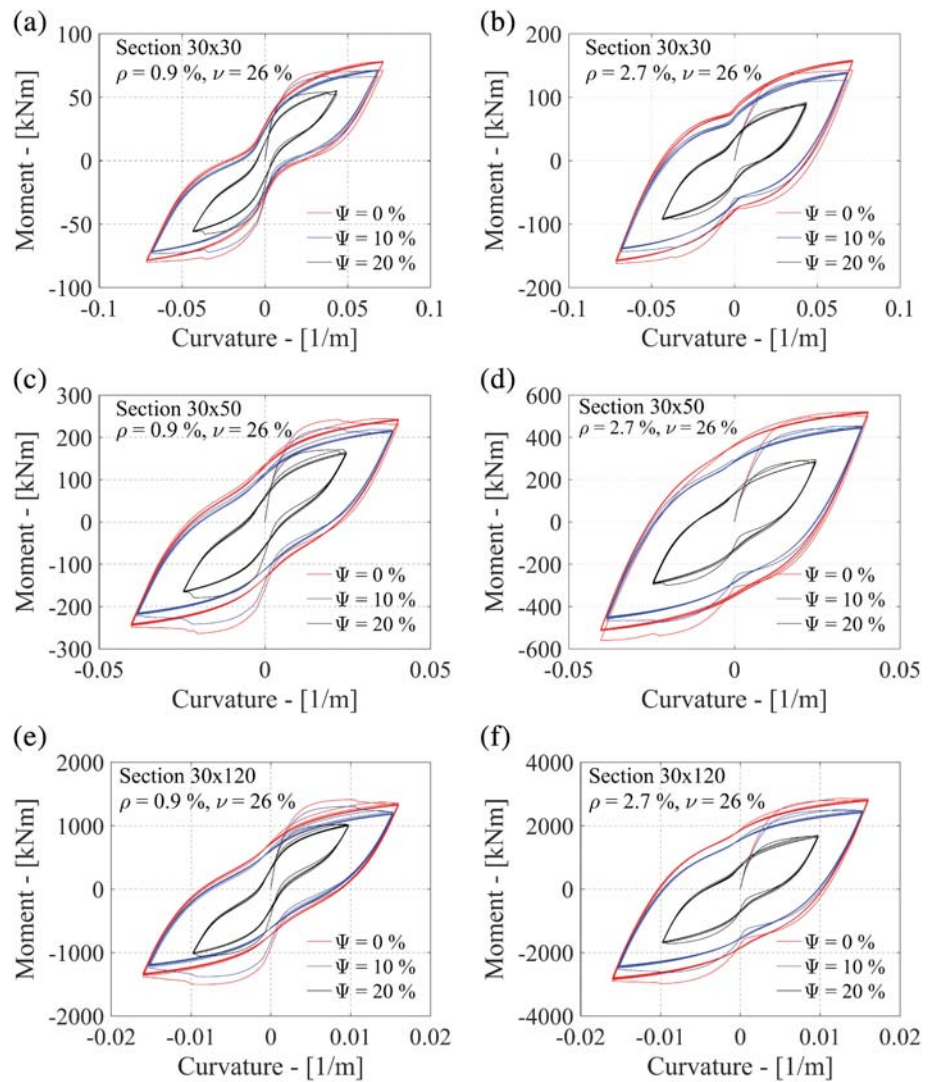


**FIGURE 11** Load History IC1. Stirrup spacing  $s = 70$  mm, Slenderness  $\lambda = 4.4$  (a),  $s = 130$  mm,  $\lambda = 8.1$  (b). Reinforcement ratio  $\rho = 0.9\%$ . Maximum strains of steel fibers for  $(\nu, \Psi, pattern)$  (ii): values of the normalized axial force  $\nu = 0, 7, 13$ , and  $26\%$ , corrosion percentage  $\Psi = 20\%$ . Rebars in compression (Comp.); Rebars in tension (Tens.); Top reinforcement (Top); Bottom reinforcements (Bot)

**FIGURE 12** IC1: Moment-curvature plots for normalized axial load  $\nu = 26\%$ ,  $L/D = 4.5$ :

- (a) section  $300 \times 300$  mm<sup>2</sup>,  $\rho = 0.9\%$ ;
- (b) section  $300 \times 300$  mm<sup>2</sup>,  $\rho = 2.7\%$ ;
- (c) section  $300 \times 500$  mm<sup>2</sup>,  $\rho = 0.9\%$ ;
- (d) section  $300 \times 500$  mm<sup>2</sup>,  $\rho = 2.7\%$ ;
- (e) section  $300 \times 1,200$  mm<sup>2</sup>,  $\rho = 0.9\%$ ;
- (f) section  $300 \times 1,200$  mm<sup>2</sup>,  $\rho = 2.7\%$



The cases with longitudinal reinforcement ratio  $\rho = 0.9\%$  and  $\rho = 2.7\%$  attain similar values of the maximum strains, therefore the former case is shown only.

We recall that the experimental tests<sup>21</sup> for the  $300 \times 300$  mm<sup>2</sup> section produced the failure of the specimen at this (estimated) curvature ductility level (for

$\Psi = 20\%$  corrosion level). The trend here obtained numerically for the three different geometries appear to be similar.

The maximum attained strains are slightly larger for section with larger height, as expected. Compressive strains are obviously smaller than the tensile ones, the former well below  $1\%$ .



Maximum strains in compression and tension reduce with corrosion. For example in the  $300 \times 300$  cross section, the maximum strains in compression are around 4.0‰, for  $\Psi = 0$  and 10%, with a light reduction in the latter, while for  $\Psi = 20\%$  the maximum strain is 3.06 ‰, corresponding to a reduction of 24%. Similar trends are observed for the sections  $300 \times 500 \text{ mm}^2$  and  $300 \times 1,200 \text{ mm}^2$  and for tensile strains.

The fact that the maximum deformations reduces with corrosion should not surprise. We recall that IC1 imposes to the section the same curvature ductility demand, this corresponds to a reduction of imposed curvature as yielding curvature reduces with corrosion. At the attained compressive strains  $\sigma$ - $\varepsilon$  model diagram is certainly very accurate.

Figure 11 gives the influence of axial force, as it shows the results of the analyses under IC1 (i.e., same curvature ductility demand) for parameter pattern (ii) in §4 (constant percentage of corrosion  $\Psi = 20\%$  and variation of the non-dimensional axial force  $\nu = 0, 7, 13$ , and 26%), stirrups spacings  $s$ : 70 mm (Figure 11a) and 130 mm (Figure 11b). The results are in terms of maximum strain of the steel rebars, both in compression and in tension.

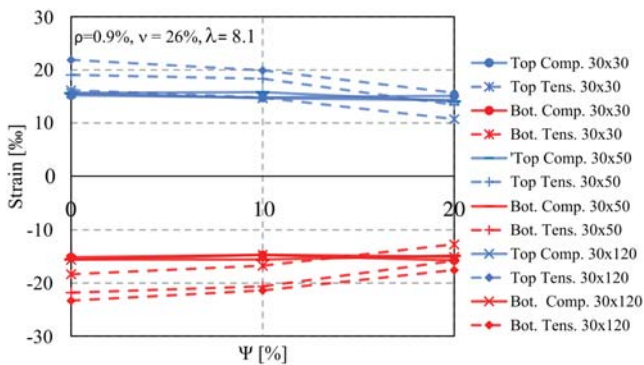


**FIGURE 13** IC2: Maximum strains of steel fibers for normalized axial load  $\nu = 26\%$ , reinforcement ratio  $\rho = 0.9\%$  and different values of the corrosion percentage:  $\Psi = 0, 10, 20\%$ : stirrup spacing  $s = 130$  mm, slenderness  $\lambda = 8.1$ . Rebars in compression (Comp.); Rebars in tension (Tens.); Top reinforcement (Top); Bottom reinforcements (Bot)

The cases with longitudinal reinforcement ratio  $\rho = 0.9\%$  and  $\rho = 2.7\%$  attain similar values of the maximum strains, therefore the former case is shown only.

It can be observed that the maximum strains in compression are smaller than 0.5%, very far from 1.5%, the higher value, for  $\nu = 26\%$ , had been shown in Figure 10. It is observed that for axial force  $\nu = 0$ , we are far from strain demand critical in tension (4%, see Figure 1).

Moment-Curvature plots for the same  $(\nu, \Psi)$  parameter pattern (ii), IC1 and slenderness  $\lambda = 4.5$  are reported in Figure 12 with left column  $\rho = 0.9$  and right column  $\rho = 2.7\%$ . We recall that for such slenderness we might have inelastic buckling for  $\Psi = 10\%$ . Buckling can be only partially appreciated in Figure 12 (c) and (d) as the compressive strains are too small to render buckling very effective. However, the case  $\Psi = 10\%$  has a larger moment reduction from yielding to the inversion, with respect to  $\Psi = 20\%$ .

In all considered sections it is possible to observe a slight reduction in terms of dissipated energy when passing from the uncorroded to the corroded section with  $\Psi = 10\%$ , while the reduction is very high for  $\Psi = 20\%$ .

Figures 13 and 14 show the results of IC2 analyses (where maximum imposed strain in steel is 1.5% in compression, as it can be seen in Figure 13)  $(\nu, \Psi)$  parameter pattern (ii), for the case  $\rho = 0.9\%$  only. The case  $\rho = 2.7\%$  gives similar results and has been omitted.

Figure 14 reports the moment-curvature plots. The imposed ductility in curvature are very high, from six to more than eight, probably beyond the section capacity limit, while we did not pose any limit in bar available ductility in this analysis.

One can observe, in Figure 13, that the obtained tensile strains corresponding to the highest curvatures imposed in this study are around 1.5–2.0% not far from steel capacity. In fact when corrosion percentages around 20% the maximum strain capacity in tension is even below 3%, see Figures 1 and 2.

We must observe that even if the sections are near failure, for the crisis of the steel in tension, those in compression are 1.5%, the imposed in IC2. At such strains in compression the experimental  $\sigma$ - $\varepsilon$  curve is linear, and the adopted cyclic model is accurate.

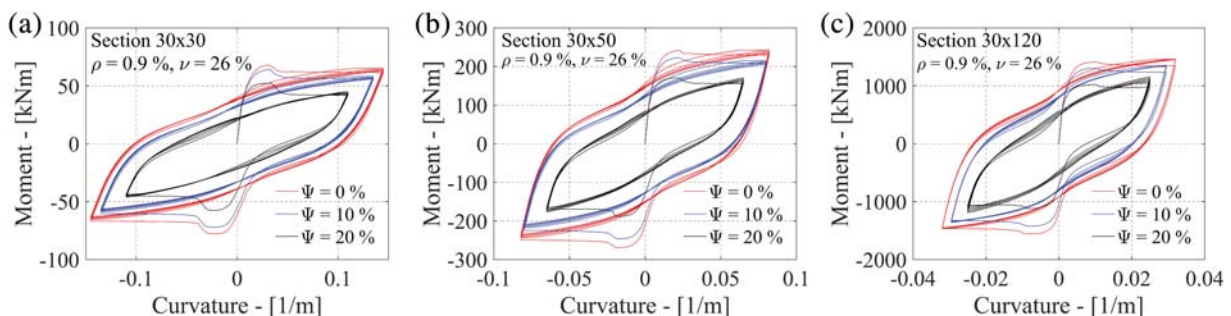


**FIGURE 14** IC2: Moment-Curvature plots for Group 2 analyses for sections for normalized axial load  $\nu = 26\%$ , slenderness  $\lambda = 8$ , reinforcement ratio  $\rho = 0.9\%$ ; (a)  $300 \times 300 \text{ mm}^2$ ; (b)  $300 \times 500 \text{ mm}^2$ ; (c)  $300 \times 1,200 \text{ mm}^2$



We may conclude that the adoption of a linear descending branch in the  $\sigma$ - $\varepsilon$  curve of rebars in presence of buckling is compatible with the effective material strain demands in reinforced concrete sections even with high corrosion percentages and very high curvature demands. Therefore, the proposed model is accurate for real fiber section analyses.

An additional interesting observation is that the reference experimental results considered in Reference 21 gave very large  $\beta_{fy}''$  values at large corrosion levels. Note that in the case of  $\Psi = 20\%$ , the reduction of the maximum resisting moment, with respect to the uncorroded case, is larger than the reduction of the area of the rebars, while for the case of  $\Psi = 10\%$  the obtained moment reduction is equal to reinforcement area reduction, around 10%. With reference to Figure 2, we already noted in §2, that other experimental works gave different results<sup>22</sup> for large  $\Psi$ 's, while at smaller values of  $\Psi$  results are similar.

## 6 | CONCLUSIONS

This paper presents numerical analyses of RC sections under cyclic bending including buckling of steel reinforcement in compression and the effects of corrosion. The steel model is the extension of the cyclic model with buckling.<sup>18</sup> All the relevant parameters of the model depend on yield strength  $f_y$ , slenderness  $\lambda$ , and the corrosion percentage  $\Psi$ . The model for buckling after yielding in Reference 18 has a linear descending branch. This is quite accurate in case the strain in compression of the rebar does not exceed 1.5%, as this is the experimental evidence.

In this paper, we have shown that these strains in compression, in usual RC sections, are much smaller than 1.5% even in case of very large ductility demands, with a numerical analysis for different sections and corrosion levels. We can therefore avoid considering a nonlinear branch after buckling, concluding that this assumption does not represent a limit and that resulting numerical simulations can be considered accurate until failure.

Three different cross sections with varying longitudinal and transversal reinforcement were chosen as case studies and were subjected to two cyclic curvature histories, the second one with very high ductility demands. One section,  $300 \times 300 \text{ mm}^2$ , corresponds to a column been tested in Reference 21. We calibrated the numerical model to reproduce the experimental results and analyzed two additional sections:  $300 \times 500$  and  $300 \times 1200 \text{ mm}^2$  with different reinforcement ratios and corrosion percentages.

The maximum compressive strains obtained in the analyses are well below 1.0%, in all the considered cases, even

for high ductility demands and high corrosion levels, within a value where the numerical rebar model is very accurate.

Once the accuracy of the model is stated the following additional conclusions can be drawn:

1. A unified model for stress strain behavior of steel including buckling allows the study of concrete sections elements and structures to evaluate their behavior with/without corrosion.
2. Corrosion reduces section strength under axial load and bending.
3. For high corrosions, strength reduction can be larger than steel area reduction.
4. Corrosion may induce longitudinal bar buckling in sections that originally were well detailed to prevent such phenomenon, as rebar slenderness increases.
5. There might be cases where, given the reduction of yield strength due to corrosion, the critical stirrup spacing increases, and buckling suitability could be reduced.
6. Dissipation is reduced as well, especially for high corrosion percentages.
7. Stirrups undergo corrosion even higher than longitudinal reinforcement as they have a lower cover with important consequences on structural behavior:
  - a. Smaller shear strength, but this is not the worst of the drawbacks.
  - b. Smaller concrete confinement.
  - c. The gap between longitudinal reinforcement and stirrups increases the free length of the longitudinal rebars and leads to premature buckling with respect to the uncorroded case. In this paper an expression is given to account for the gap, but this aspect needs further research and can be investigated experimentally and numerically.
  - d. In case of stirrup breakage, the consequences could be dramatic. Obviously, in case of stirrup breakage caused by corrosion, the increase of  $L'$  (free length  $L$  after corrosion) would be very high as, at least on the section side of stirrup failure, the free length of longitudinal bars doubles if stirrups are equally spaced. Stirrup breakage happens for high corrosion only, while on the other hand, the gap with longitudinal rebars is created at any level of corrosion.
8. The effect of low cycle fatigue can be included but is not considered here given the scope of the paper.

The inclusion of the nonlinear branch in the compression model when buckling happens and for very high deformations is possible. However, it does not allow to have a unified model for steel, including buckling and corrosion. It has been shown that it is not relevant for practical cases.

It is a matter of fact that large uncertainties exist for the calibration of corroded steel models. Part of the

uncertainties are random but large part are epistemic. The random part can be treated via Monte Carlo analyses using efficient models like the one at hand.

The authors want to stress the concept that 1.5% strain in compression is hardly overtaken in real cases, therefore the unified model represents a powerful and efficient tool for concrete sections under extreme environmental situations including large seismic actions.


The parameters of the “corroded” steel models were calibrated on the base of literature tests, though the number of meaningful tests is limited and further experimental investigations are recommended.

## ACKNOWLEDGMENTS

The authors gratefully acknowledge the DPC-ReLUIS consortium for the financial support within the framework of the 2014–2018 and of the 2019–2021 Research Projects.

## ORCID

*Davide Lavorato*  <https://orcid.org/0000-0001-7753-1975>

*Gabriele Fiorentino*  <https://orcid.org/0000-0002-6444-0473>

*Alessandro Rasulo*  <https://orcid.org/0000-0003-4911-1812>

*Alessandro Vittorio Bergami*  <https://orcid.org/0000-0002-7761-2190>

*Bruno Briseghella*  <https://orcid.org/0000-0002-8002-2298>

*Camillo Nuti*  <https://orcid.org/0000-0002-0385-201X>

## REFERENCES

- Broomfield JP. Corrosion of steel in concrete: Understanding, investigation and repair. 2nd ed. London, CRC Press, 2006.
- Castel A, François R, Arliguie G. Mechanical behaviour of corroded reinforced concrete beams-part 1: Experimental study of corroded beams. *Mater Struct*. 2000;33(9):539–544.
- Coronelli D, Gambarova P. Structural assessment of corroded reinforced concrete beams: Modeling guidelines. *J Struct Eng*. 2004;130(8):1214–1224.
- Bertolini L, Elsener B, Pedferri P, Redaelli E, Polder R. Corrosion of steel in concrete. Vol 392. Weinheim, Germany: Wiley, 2013.
- Kashani MM, Lowes LN, Crewe AJ, Alexander NA. Finite element investigation of the influence of corrosion pattern on inelastic buckling and cyclic response of corroded reinforcing bars. *Eng Struct*. 2014;75:113–125.
- Du YG, Clark LA, Chan AHC. Effect of corrosion on ductility of reinforcing bars. *Mag Concr Res*. 2005;57(7):407–419.
- Cairns J, Plizzari GA, Du Y, Law DW, Franzoni C. Mechanical properties of corrosion-damaged reinforcement. *ACI Mater J*. 2005;102(4):256.
- Apostolopoulos A, Matikas TE. Corrosion of bare and embedded in concrete steel bar–impact on mechanical behavior. *Int J Struc Integ*. 2016;7(2):240–259.
- Zhang R, Castel A, François R. Concrete cover cracking with reinforcement corrosion of RC beam during chloride-induced corrosion process. *Cem Concr Res*. 2010;40(3):415–425.
- Kashani MM, Lowes LN, Crewe AJ, Alexander NA. Phenomenological hysteretic model for corroded reinforcing bars including inelastic buckling and low-cycle fatigue degradation. *Comput Struct*. 2015;156:58–71.
- Di Carlo F, Meda A, Rinaldi Z. Numerical cyclic behaviour of un-corroded and corroded RC columns reinforced with HPFRc jacket. *Compos Struct*. 2017;163:432–443.
- Xue J, Lavorato D, Bergami AV, et al. Severely damaged reinforced concrete circular columns repaired by turned steel rebar and high-performance concrete jacketing with steel or polymer fibers. *App Sci (Switzerland)*. 2018;8(9):1–33. <https://doi.org/10.3390/app8091671>
- Lavorato D, Bergami AV, Fiorentino G, Fiore A, Santini S, Nuti C. Experimental tests on existing RC beams strengthened in flexure and retrofitted for shear by C-FRP in presence of negative moments. *Int J Adv Struc Engine*. 2018;10(3):211–232.
- Lavorato, D., Nuti, C., Santini, S., Briseghella, B., & Xue, J. (2015). A repair and retrofitting intervention to improve plastic dissipation and shear strength of Chinese RC bridges. In IABSE Symposium Report (Vol. 105, No. 9, pp. 1–6). International Association for Bridge and Structural Engineering.
- Lavorato D, Nuti C, Santini S. Experimental investigation of the shear strength of RC beams extracted from an old structure and strengthened by carbon FRP u-strips. *Appl Sci*. 2018;8(7):1182.
- Forte, A., Santini, S., Fiorentino, G., Lavorato, D., Bergami, A. V., Nuti, C. (2018), Influence of materials knowledge level on the assessment of the shear strength characteristic value of existing RC beams, Proceedings of the 12th fib international PhD symposium in Civil Engineering, pp. 979–986.
- The MathWorks, Inc., MA, USA. Version R2018a.
- Monti G, Nuti C. Nonlinear cyclic behavior of reinforcing bars including buckling. *J Struct Eng*. 1992;118(12):3268–3284.
- Zhou, Z., Nuti, C., & Lavorato, D. (2014). Modeling of the mechanical behavior of stainless reinforcing steel. In Proceedings of the 10th fib International, PhD Symposium in Civil Engineering, Université Laval, QC, Canada (pp. 21–23).
- Zhou, Z., Lavorato, D., Nuti, C., & Marano, G. C. (2015). A model for carbon and stainless steel reinforcing bars including inelastic buckling for evaluation of capacity of existing structures. In Proceedings of the 5th ECCOMAS Thematic Conference on Computational Methods in Structural Dynamics and Earthquake Engineering, Crete Island, Greece (pp. 25–27).
- Meda A, Mostosi S, Rinaldi Z, Riva P. Experimental evaluation of the corrosion influence on the cyclic behaviour of RC columns. *Eng Struct*. 2014;76:112–123.
- François R, Khan I, Dang VH. Impact of corrosion on mechanical properties of steel embedded in 27-year-old corroded reinforced concrete beams. *Mater Struct*. 2013;46(6):899–910.
- Kashani MM, Crewe AJ, Alexander NA. Nonlinear cyclic response of corrosion-damaged reinforcing bars with the effect of buckling. *Constr Build Mater*. 2013;41:388–400.
- Zhou, Z. (2015), Uniaxial material model for reinforcing Bar including buckling in RC structures, PhD dissertation, Department of Engineering, Roma Tre University, June 2015.
- Menegotto M, Pinto PE. Method of analysis for cyclically loaded reinforced concrete plane frames including changes

in geometry and non-elastic behaviour of elements under combined normal force and bending. IABSE symposium of resistance and ultimate deformability of structures acted on by well-defined repeated loads. Volume 13. Portugal: International Association of Bridge and Structural Engineering, Lisbon, 1973; p. 15–22.

26. Dahkal RP, Maekawa K. Modeling for Postyield buckling of reinforcement. *J Struct Eng*. 2002;128(9):1253–1262.
27. Scott BD, Park R, Priestley MJN. Stress-strain behavior of concrete confined by overlapping hoops at low and high strain rates. *Am Concr Inst J*. 1982;79(1):13–27.
28. CEN, 2005. Eurocode 8: Design of structures for earthquake resistance. Part 2: Bridges final draft prEN 1998–2, European Committee for Standardization, Brussels, Belgium.
29. Sheikh, M. N., Tsang, H. H., McCarthy, T. J., & Lam, N. T. K. (2010). Yield curvature for seismic design of circular reinforced concrete columns.

## AUTHOR BIOGRAPHIES



Davide Lavorato, Associate Professor Department of Architecture, Roma Tre University, Largo G. B. Marzi 10, 00153, Roma, Italy. Email: [davide.lavorato@uniroma3.it](mailto:davide.lavorato@uniroma3.it)



Gabriele Fiorentino, Research Associate, Department of Architecture, Roma Tre University, Largo G. B. Marzi 10, 00153, Roma, Italy. Email: [gabriele.fiorentino@uniroma3.it](mailto:gabriele.fiorentino@uniroma3.it)



Angelo Pelle, PhD Student, Department of Architecture, Roma Tre University, Largo G. B. Marzi 10, 00153, Roma, Italy. Email: [angelo.pelle@uniroma3.it](mailto:angelo.pelle@uniroma3.it)



Alessandro Rasulo, Assistant Professor, Department of Civil and Mechanical Engineering, University of Cassino and Southern Lazio, Via Gaetano di Biasio, 43, 03043 Cassino, Italy. Email: [a.rasulo@unicas.it](mailto:a.rasulo@unicas.it)



Alessandro Vittorio Bergami, Assistant Professor, Department of Architecture, Roma Tre University, Largo G. B. Marzi 10, 00153, Roma, Italy. Email: [alessandro.bergami@uniroma3.it](mailto:alessandro.bergami@uniroma3.it)



Bruno Briseghella, Full Professor and Dean, College of Civil Engineering, Fuzhou University, 2 Xue Yuan Road, University Town, Fuzhou, Fujian 350108, PR China. Email: [bruno@fzu.edu.cn](mailto:bruno@fzu.edu.cn)



Camillo Nuti, Full Professor, Department of Architecture, Roma Tre University, Largo G. B. Marzi 10, 00153, Roma, Italy. Email: [camillo.nuti@uniroma3.it](mailto:camillo.nuti@uniroma3.it)

## SUPPORTING INFORMATION

Additional supporting information may be found online in the Supporting Information section at the end of this article.

**How to cite this article:** Lavorato D, Fiorentino G, Pelle A, et al. A corrosion model for the interpretation of cyclic behavior of reinforced concrete sections. *Structural Concrete*. 2020;1–15. <https://doi.org/10.1002/suco.201900232>